A Recoil-Carbon Polarimeter for the Booster Ring at BNL

Frank Rathmann, Vera Shmakova, Evgeny Shulga, and al.

Brookhaven National Laboratory, Upton, New York 11973, USA

March 20, 2026

Why polarimetry in the Booster?

- The BNL Booster accelerates the polarized proton beam from Linac injection ($\sim$200 MeV) to extraction ($\sim$1.5 GeV)
- Also accelerates the polarized $^3\mathrm{He}$ ion beam from EBIS at $T_{\mathrm{inj}}^{^3\mathrm{He}} = 6$ MeV to 2497 MeV at extraction
- Polarimetry required to monitor and optimize polarization during acceleration from injection to extraction
- Polarimeter concept: elastic scattering from a carbon target, detect the recoil $^{12}\mathrm{C}$ nuclei
  - $p + {}^{12}\mathrm{C} \to p + {}^{12}\mathrm{C}$
  - $^3\mathrm{He} + {}^{12}\mathrm{C} \to {}^3\mathrm{He} + {}^{12}\mathrm{C}$
- **Key requirement**: fixed detector geometry must provide continuous coverage over the full energy range — no mechanical adjustment

BNL Booster Parameters

Proton beam vs. ^{3}He ion beam

Quantity	Symbol	Unit	Proton beam	^{3}He ion beam
Rest mass	m	MeV/c^2	938.272	2808.39
Charge state	q	e	$+1$	$+2$
Anomalous magnetic moment	G	–	1.792847	-4.1842
Injection kinetic energy	T_{inj}	MeV (MeV/u)	200	6 (2)
Extraction kinetic energy	T_{extr}	MeV (MeV/u)	1500	2497 (832)
Injection momentum	p_{inj}	MeV/c	644	184
Extraction momentum	p_{extr}	MeV/c	2251	4501
Injection magnetic rigidity	$B\rho_{\mathrm{inj}}$	T·m	2.150	0.306
Extraction magnetic rigidity	$B\rho_{\mathrm{extr}}$	T·m	7.507	
Injection revolution frequency	$f_{\mathrm{rev,inj}}$	MHz	0.841	0.097
Extraction revolution frequency	$f_{\mathrm{rev,extr}}$	MHz	1.371	1.261
Injection spin tune	$\nu_{s,\mathrm{inj}} = G\gamma_{\mathrm{inj}}$	–	$+2.175$	-4.193
Extraction spin tune	$\nu_{s,\mathrm{extr}} = G\gamma_{\mathrm{extr}}$	–	$+4.659$	-7.904
Repetition frequency	f_{rep}	Hz	7.5	1
Repetition period	$T_{\mathrm{rep}} = 1/f_{\mathrm{rep}}$	ms	133	1000
Acceleration ramp time	T_{ramp}	ms	≈ 75	≈ 75
Bunches per cycle	n_b	–	1	1
Intensity per bunch	N_b	10^{11}	1.5	1.0 (2.5 design)
Intensity per cycle	$N_{\mathrm{cyc}} = n_b\, N_b$	10^{11}	1.5	1.0 (5.0 design)

Elastic Scattering Kinematics

Recoil Angle vs. Projectile Angle

pC and ^{3}He C elastic scattering at injection and extraction energies

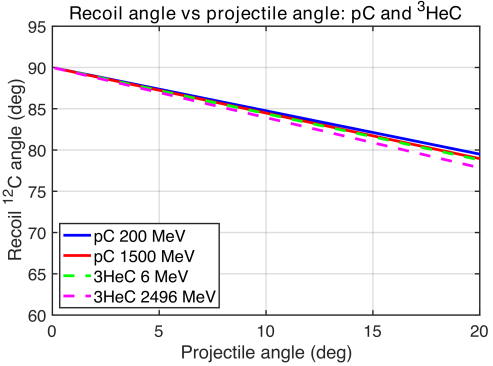

Recoil ^{12}C Angle

- ^{12}C mass $\gg$ projectile mass $\Rightarrow$ recoil nuclei emerge predominantly at large lab angles:

$$\theta_C \approx 70^\circ\text{–}90^\circ$$

- Nearly independent of beam species and energy
- $\Rightarrow$ **Fixed recoil detector geometry** provides continuous coverage — no mechanical adjustment
- Forward angles: $\theta \approx 5^\circ$–20°

Recoil Carbon Kinetic Energy vs. Recoil Angle

Full Booster energy range — pC and $^3\mathrm{He}\,C$

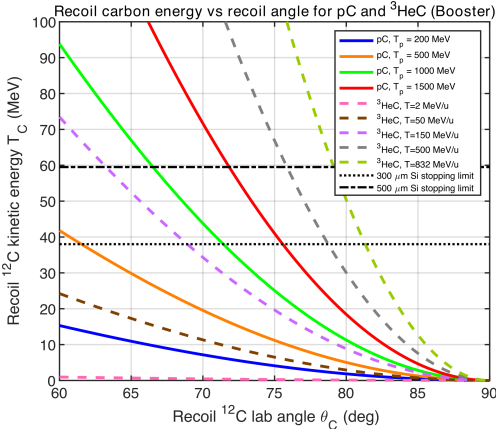

Recoil Energies

- Proton recoil: sub-MeV (inj.) to $\lesssim 60\,\mathrm{MeV}$ (extr.)
- $^3\mathrm{He}$ recoil: up to $\sim 90\,\mathrm{MeV}$ at highest energies
- Detector thickness:
  - 300 µm stops recoil carbon nuclei over most of the angular range for protons and over a large fraction of the angular range for the ^{3}He
  - 500 µm stops essentially the complete relevant recoil angular range

Existing Data

pC Elastic Scattering — Data & Parametrization (Bonin et al.)

McNaughton + Bonin parametrization covers the full Booster energy range

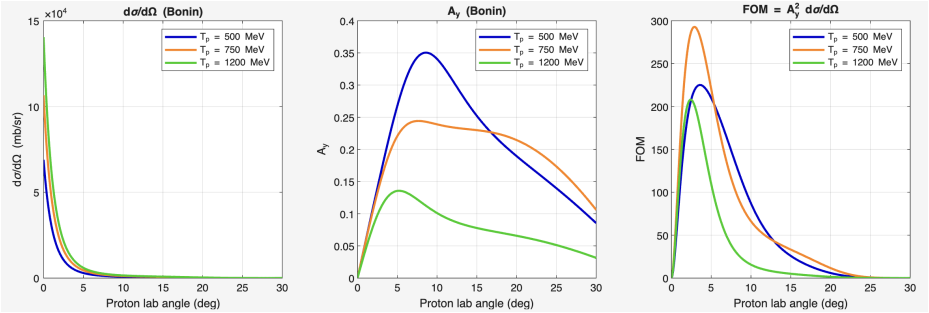

- Elastic pC data and A_y exist over the full Booster energy range, including energies up to and beyond 1.5 GeV
- Bonin et al. parametrization covers $p = 1.0\,\mathrm{GeV/c}$ to $1.9\,\mathrm{GeV/c}$: $A_y(\theta, p)$ and $d\sigma/d\Omega(\theta, p)$
- Figure of merit: $\mathrm{FOM}(\theta) = A_y^2(\theta)\,\frac{d\sigma}{d\Omega(\theta)}$
  - Statistical precision: $\delta P \propto 1/\sqrt{I\, d_t\, \Delta\Omega\, t\, \mathrm{FOM}}$
- FOM has broad maximum defines the optimal angular region for detector placement

$^3\mathrm{He}\,\mathrm{C}$ Elastic Scattering Data — The 443 MeV Anchor (Kamiya et al.)

The only experimental anchor in the Booster energy range

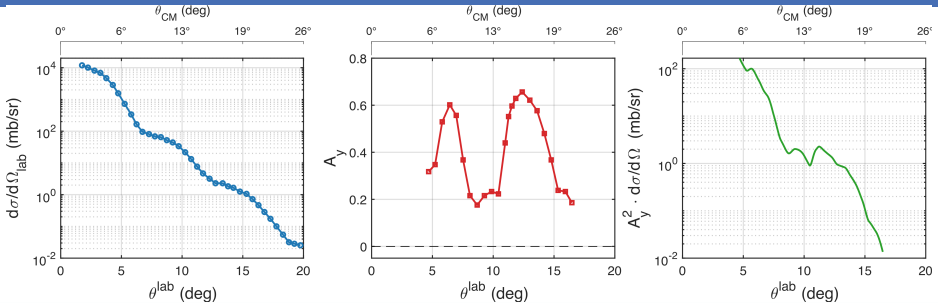

- Kamiya et al. (Phys. Rev. C **67**, 2003): measured $d\sigma/d\Omega$ and induced polarization for elastic $^3\mathrm{He} + {}^{12}\mathrm{C}$ at 443 MeV
- **Key result**: A_y reaches maximum ≈ 0.63 near $\theta_{\mathrm{lab}} \approx 8°$–$9°$
- Kinematic conversion CM $\rightarrow$ lab via relativistic two-body kinematics:
  - Invariant mass $\sqrt{s} = 14\,322$ MeV
  - CM frame velocity $\beta_{\mathrm{cm}} = 0.1134$
  - Velocity ratio $r = \beta_{\mathrm{cm}}/\beta_p = 0.273 < 1$
  - $r < 1 \Rightarrow$ unique one-to-one mapping between CM and lab angles over the full angular range

dC Elastic Scattering

Nucleus	I	μ (μ_N)	$g = A\mu/(ZI\mu_N)$	G
p	$\frac{1}{2}$	$+2.7928$	$+5.5856$	$+1.7928$
^{3}He	$\frac{1}{2}$	-2.1276	-6.3828	-4.1914
d	1	$+0.8574$	$+1.7148$	-0.1426
^{6}Li	1	$+0.8220$	$+1.6440$	-0.1780
^{7}Li	$\frac{3}{2}$	$+3.2564$	$+5.0648$	$+1.5324$

Stone, Atomic Data and Nucl. Data Tables, 90(1):75–176, 2005; p and d from Tiesinga et al., Rev. Mod. Phys., 93:025010, 2021.

dC analyzing power data across the Booster range

- Satou et al., Physics Letters B, 549(3):307–313, 2002 (270 MeV, RCNP)
- Müller et al. , The European Physical Journal A, 56(8):211, Aug 2020 (COSY)
- Müller et al.,Journal of Instrumentation, 15(12):P12005, 2020 (COSY)
- These datasets together establish the dC data basis as **comparable in quality to the pC case**, covering the full Booster energy range

Deuteron: uniquely favourable spin dynamics

$G_d = -0.1426$ is unusually small: the spin tune $\nu_s = G_d\gamma$ stays $\ll 1$ throughout the **entire** Booster cycle. Neither imperfection ($\nu_s = k$) nor intrinsic ($\nu_s = kP \pm Q_{x,y}$) resonances are crossed — polarized deuterons need no resonance mitigation.

^{6,7}Li+C Elastic Scattering

- Both isotopes have pronounced α-cluster structure: $^6\mathrm{Li} \approx \alpha + d$, $^7\mathrm{Li} \approx \alpha + t$
  The α core carries no spin; nuclear magnetic properties dominated by the d or t cluster
- ^{6}Li ($I = 1$):
  $G_{^6\mathrm{Li}} = -0.178 \approx G_d = -0.143$ — d-cluster dominates the magnetic moment
- ^7Li ($I = \frac{3}{2}$):
  $G_{^7\mathrm{Li}} = +1.532 \approx G_p = +1.793$ — $I = 1$ orbital motion of t around α core does not cancel, giving large G
- ^6Li: small $|G| \Rightarrow$ few depolarizing resonances, similarly favourable to the deuteron; polarization transport from source well controlled
- ^7Li: $G \approx G_p \Rightarrow$ resonance density comparable to the proton; analogous harmonic-correction and AC-dipole strategies required

Data situation — no Booster-range A_y data exist

- ^6Li**+C:** vector A_y measured only up to 150 MeV (Tanaka et al., 1987) — no data in the Booster energy range
- ^7Li**+C:** only *unpolarized* $d\sigma/d\Omega$ at intermediate energies (Nadasen et al., 1995) — no A_y data at any Booster-relevant energy
- The Booster polarimeter is therefore identified as the instrument to **map LiC analyzing powers across the full Booster ramp**, in direct analogy to the role foreseen for ^{3}HeC (Sec. 3.3)

Detector: same geometry, extended physics reach

- Fixed recoil ring covers LiC kinematics **without modification** — confirmed by Fig. 1 (bottom-right panel); kinematic arguments depend only on projectile-to-carbon mass ratio and $B\rho$
- ^6Li ($I = 1$): six stations resolve A_y and A_{yy} simultaneously via $\cos\phi$ and $\cos 2\phi$
- ^7Li ($I = \frac{3}{2}$): higher-rank tensor moments in principle accessible with the same geometry

Polarimeter Design

Detector concept, geometry, and kinematic event selection

- Transverse beam polarization extracted from azimuthal asymmetry:

$$\frac{dN}{d\phi} \propto 1 + P_y\, A_y \cos\phi$$

  where P_y = vertical polarization, ϕ = azimuthal angle of recoil
- $p\mathrm{C}$ elastic: **recoil ring alone** is sufficient for clean elastic event selection
  - Measured (θ_C, T_C) pair on the elastic locus identifies event
  - No forward detector required for $p\mathrm{C}$ polarimetry
- $^3\mathrm{He}\,\mathrm{C}$ elastic: **forward coincidence is essential**
  - $^3\mathrm{He}$ binding energy only 7.72 MeV — breakup (p+d, p+p+n) is accessible at all Booster energies
  - Recoil carbon from breakup can mimic elastic recoils — indistinguishable from recoil alone
  - Forward $^3\mathrm{He}$ detection in coincidence resolves ambiguity: two-body kinematics uniquely relate θ and θ_C for elastic events
  - Breakup events violate two-body constraint $\Rightarrow$ rejected by the coincidence condition

Side View: Overall Detector Layout (r–z plane)

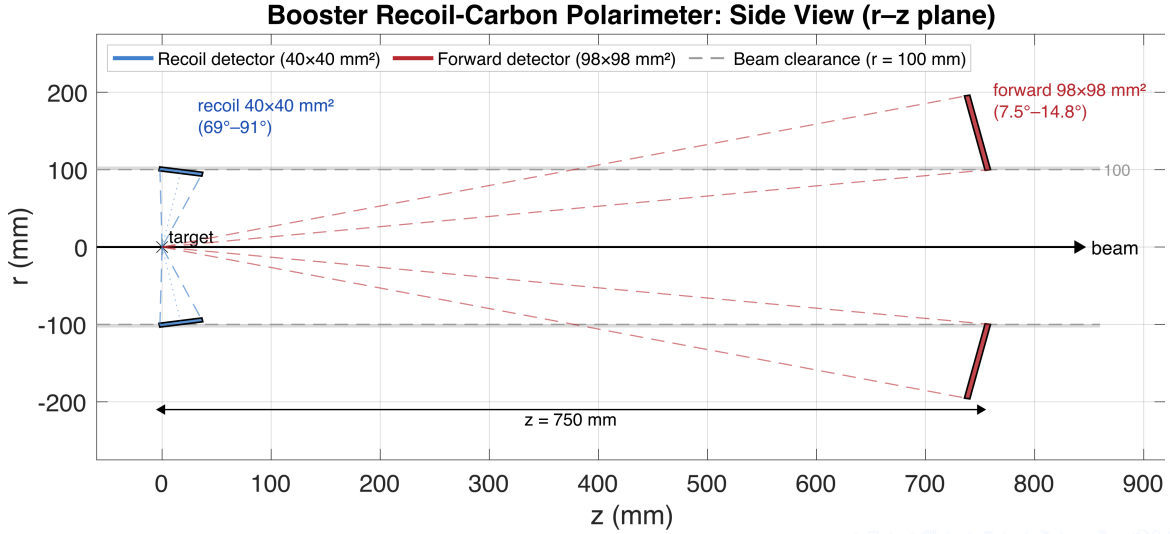

Recoil Detector Ring

Six $40 \times 40\,\mathrm{mm}^2$ silicon pad stations at $r = 100\,\mathrm{mm}$, $z = 17.6\,\mathrm{mm}$

Geometry

- 6 stations at 60° azimuthal spacing
- Radial center: $r = 100\,\mathrm{mm}$, $z = 17.6\,\mathrm{mm}$
- Face center at $\theta_C = \arctan(100/17.6) = 80°$
- Face edges at $\theta_C = 68.9°$–$91.2°$ ($\Delta\theta_C = 22.3°$)
- Face tilted $\perp$ to recoil at 80°

Detector Specs

- $40 \times 40\,\mathrm{mm}^2$ silicon pad, 500 µm thick
- 500 µm stops $^{12}\mathrm{C}$ up to $\sim 59\,\mathrm{MeV}$ ($p\mathrm{C}$: full stopping for $\theta_C \gtrsim 73°$)
- For $^{3}\mathrm{He}\,\mathrm{C}$ at extraction: ΔE element
- Strips run radially: provide ϕ within $\pm 30°$
- θ_C from T_C via kinematic relation

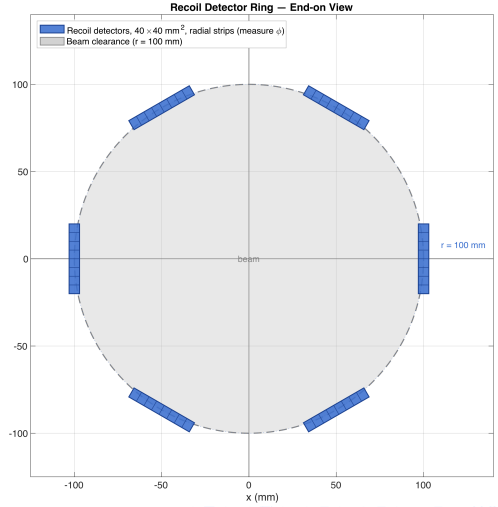

Forward Detector Ring

Six $98 \times 98\,\mathrm{mm}^2$ Hamamatsu silicon pads at $z = 750\,\mathrm{mm}$

Geometry

- 6 stations at same azimuthal positions as recoil ring
- $z = 750\,\mathrm{mm}$ downstream of target
- Inner edge: $r = 100\,\mathrm{mm}$, outer edge: $r = 198\,\mathrm{mm}$
- Angular acceptance: $\theta = 7.6^\circ$–14.8°

Detector Specs & Physics

- $98 \times 98\,\mathrm{mm}^2$ Hamamatsu, $320\,\mu\mathrm{m}$ thick
- Strips run azimuthally: provide θ resolution for coincidence
- $\theta = 7.6^\circ$–14.8° covers FOM maximum for $^3\mathrm{He}\,\mathrm{C}$ at 443 MeV (A_y peaks at $\theta \approx 8^\circ$–9°)
- Same range covers large-FOM region for $p\mathrm{C}$
- $\Omega_{\mathrm{fwd}} = 6 \times 0.026\,\mathrm{sr} = 0.15\,\mathrm{sr}$ (1.2% of 4π)

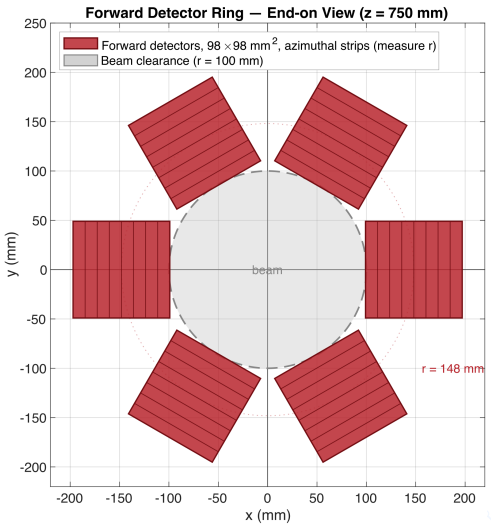

$^3\mathrm{He}\,C$ Forward Coincidence Window

Recoil angle θ_C vs. forward $^3\mathrm{He}$ angle θ_{fwd} across the Booster ramp

	θ_C (°)			
θ_{fwd} (°)	$T = 6$ MeV	$T = 450$ MeV	$T = 1500$ MeV	$T = 2496$ MeV
7	85.6	85.5	85.2	84.8
9	84.4	84.2	83.8	83.4
11	83.1	82.9	82.4	81.9
13	81.9	81.6	81.0	80.5
15	80.6	80.3	79.7	79.0

All θ_C values fall within the recoil ring acceptance (68.9°–91.2°), confirming coincidence coverage across the full ramp.

θ_C varies by less than 1° from injection to extraction for a given θ_{fwd}. Effective coincidence window: $\theta_C \approx 79°$–$86°$.

Provision for Deuteron Polarimetry

Blank flanges at $z = 400\,\text{mm}$ for a future $d\text{C}$ forward ring

- Six-station geometry supports spin-1 deuteron polarimetry:

$$\frac{dN}{d\phi} \propto 1 + \tfrac{3}{2} A_y p_y \cos\phi + \tfrac{1}{2} A_{yy} p_{yy} (\cos^2\phi - \tfrac{1}{3}) + \cdots$$

- Six stations resolve both $\cos\phi$ (vector p_y) and $\cos 2\phi$ (tensor p_{yy}) modulations
- At $B\rho = 7.507\,\text{T m}$: $T_d = 1054\,\text{MeV}$ (527 MeV/u) — same momentum as proton at 1.5 GeV
- $d\text{C}$ forward angles $\theta_d = 14°$–$34°$ for $\theta_C = 69°$–$82°$ — entirely **above** the ^3He forward ring acceptance (7.6°–14.8°)
  - Existing ^3He forward ring at $z = 750\,\text{mm}$ provides **no** useful coincidence coverage for $d\text{C}$ scattering
- **Solution**: blank flanges at $z = 400\,\text{mm}$ at the azimuthal positions of the existing forward stations
  - $\theta_d = 14°$–$34°$ maps to $r = 100$–$270\,\text{mm}$ at $z = 400\,\text{mm}$: coverable by two $98 \times 98\,\text{mm}^2$ pads
  - $d\text{C}$ ring does **not** shadow the ^3He forward ring
  - Blank flanges add no material to ^3He forward acceptance

Forward Deuteron Angles at $z = 400\,\text{mm}$

Elastic dC at Booster extraction energy $T_d = 1054\,\text{MeV}$

θ_C (°)	θ_d (°)	T_C (MeV)
69	33.7	73.1
71	30.4	60.3
73	27.2	48.6
75	23.9	38.1
77	20.7	28.8
79	17.5	20.7
81	14.3	13.9
83	11.1	8.5
85	7.9	4.3

The bulk of useful acceptance ($T_C \gtrsim 10\,\text{MeV}$, $\theta_C \lesssim 82°$) maps to $\theta_d \approx 14°$–$34°$. Quantitative performance evaluation is deferred to a future study pending availability of dC A_y data.

Polarization Measurement Performance

Beam-Target Overlap & IPM Beta Functions

Geometric overlap fraction f_{ov} between beam and carbon fibre

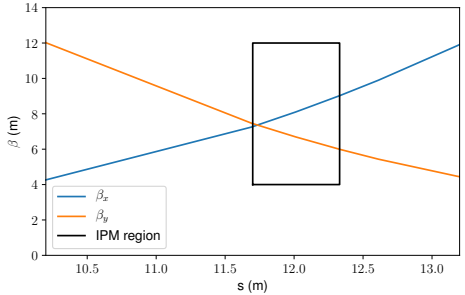

Beam & Target

- $\beta_x \approx \beta_y \approx 7.75\,\mathrm{m} \Rightarrow$ round beam
- $\sigma \approx 3.4\,\mathrm{mm}$ (inj.) to $1.8\,\mathrm{mm}$ (extr.)
- $d_t = 4\,\mu\mathrm{g/cm}^2, \quad d_{\mathrm{fibre}} \approx 18\,\mathrm{nm}$
- $f_{\mathrm{ov}} = \mathrm{erf}(d_{\mathrm{fibre}}/2\sqrt{2}\,\sigma_x) \sim 10^{-6}$

Table 11: Geometric overlap fraction f_{ov}

Species	T (MeV)	$\beta\gamma$	σ (mm)	f_{ov}
p	500	1.162	2.58	1.24×10^{-4}
p	850	1.623	2.19	1.46×10^{-4}
p	1200	2.048	1.95	1.64×10^{-4}
$^3\mathrm{He}$	443	0.583	3.65	0.87×10^{-4}

$$f_{\mathrm{ov}} = \underbrace{\int_{-d_{\mathrm{fiber}}/2}^{+d_{\mathrm{fiber}}/2} \frac{1}{\sqrt{2\pi}\,\sigma_x} e^{-x^2/2\sigma_x^2}\,dx}_{\text{narrow direction}} \cdot \underbrace{\int_{-\infty}^{\infty} \frac{1}{\sqrt{2\pi}\,\sigma_y} e^{-y^2/2\sigma_y^2}\,dy}_{=1}$$

Dwell Time for $\delta P = 2 \times 10^{-2}$

*p*C: within one ramp cycle; ^{3}He C: multiple cycles needed

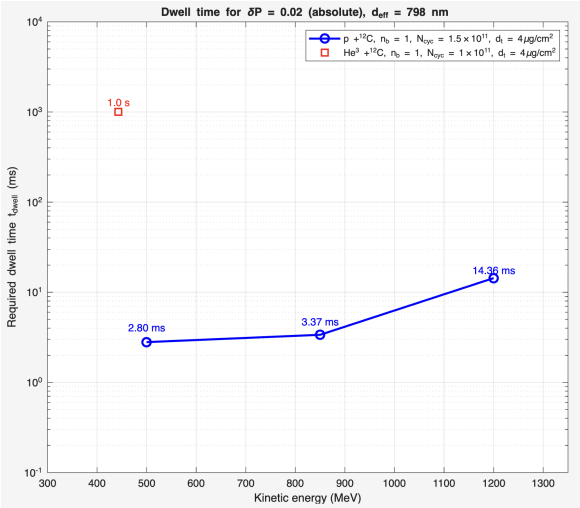

*p*C (blue circles)

- FOM: ∼3000 → ∼800 mb/sr (500–1200 MeV)
- t_{dwell}: 3 ms to 15 ms — well within 75 ms ramp
- Statistics-free in one cycle

^{3}He C (red square)

- FOM ≈ 12 mb/sr (at 443 MeV)
- $t_{\mathrm{dwell}} \approx 1\,\mathrm{s} \Rightarrow$ many ramp cycles needed

$$t_{\mathrm{dwell}} = \frac{1}{N_{\mathrm{cyc}}\, f_{\mathrm{rev}}\, \frac{d_t N_A}{A_C}\, f_{\mathrm{ov}}\, \Delta\Omega\, \mathrm{FOM}\, (\delta P)^2}$$

Detector Counting Rates & Operating Modes

Rate analysis, strip occupancy, and operating strategy for pC and $^{3}\mathrm{He}$ C

Counting Rates: Context and Instantaneous Rate

Short dwell times ⇒ high instantaneous rates — the key challenge

Why rates matter

- Dwell times are far shorter than the ramp ($\ll 75$ ms)

⇒ Statistical precision is easy — but the detector must handle the implied **instantaneous counting rate**

- Pile-up in a single readout channel degrades energy resolution and corrupts the T_C–θ_C elastic identification
- The rate problem **must** be solved in the detector system
- Neither reducing N_{cyc} nor moving the target faster is a valid solution

Instantaneous elastic rate

$$R(x_0) = N_{\mathrm{cyc}}\, f_{\mathrm{rev}}\, n_t\, f_{\mathrm{ov}}(x_0)\, \frac{d\sigma}{d\Omega}\, \Delta\Omega$$

- $f_{\mathrm{ov}}(x_0)$ depends only on fiber *position*, not speed — moving the target faster **does not** reduce the instantaneous rate
- Reducing N_{cyc} is excluded on physics grounds: polarimetry must reflect true machine conditions (space charge, depolarization resonances are intensity-dependent)

Strip Segmentation and Per-Strip Occupancy

128-strip sensors divide rate by 128 — the practical rate mitigation

Sensor segmentation

- **Recoil ring**: 128 *azimuthal* strips per station
  - Subdivides 60° azimuthal coverage
  - $\Delta\phi \approx 0.47^\circ$ per strip
- **Forward ring**: 128 *radial* strips per station
  - Subdivides $r = 100$–198 mm
  - $\Delta r \approx 0.77$ mm per strip
  - Provides θ resolution for coincidence constraint

Occupancy per strip

$$\mathcal{O} = R_{\text{strip}} \times \tau_{\text{shape}}$$

- $\mathcal{O} \ll 1$ required to avoid pile-up degrading energy resolution and elastic ID

Key conclusion

Rate per strip $= R_{\text{station}}/128$ — strip readout is the primary mechanism for keeping occupancy manageable.

Counting Rate Summary

Per-station and per-strip rates for pC (singles & coincidence) and ^{3}He C (coincidence)

Species	Mode	T (MeV)	f_{ov}	$\langle d\sigma/d\Omega\rangle$ (mb/sr)	$\langle A_y\rangle$	$\langle \mathrm{FOM}\rangle$ (mb/sr)	R/stn	R/strip	$\mathcal{O}_{100}$ (10^{-3})
pC	singles	500	1.2×10^{-4}	52 800	0.22	2 890	88 MHz	688 kHz	69
		850	1.5×10^{-4}	81 600	0.21	3 760	181 MHz	1.4 kHz	141
		1200	1.6×10^{-4}	107 500	0.08	660	282 MHz	2.2 kHz	220
pC	coinc.	500	1.2×10^{-4}	57 900	0.31	5 630	6.3 MHz	49 kHz	4.9
		850	1.5×10^{-4}	89 400	0.24	4 980	12.9 MHz	101 kHz	10
		1200	1.6×10^{-4}	117 900	0.09	1 050	20 MHz	158 kHz	16
^{3}HeC	coinc.	443	0.87×10^{-4}	30	0.63	12	1 kHz	8 Hz	$<10^{-5}$

$\mathcal{O}_{100}$: occupancy per strip at $\tau_{\mathrm{shape}} = 100$ ns. pC from Bonin parametrization; ^{3}HeC from Kamiya et al. at 443 MeV. Beam parameters from Table 1; $d_t = 4\,\mu\mathrm{g/cm}^2$.

$^{3}\mathrm{He}\,\mathrm{C}$ at Booster Energies: Uncharted Territory

Above 450 MeV — unknown A_y; strategy for determination

^{3}He C Above 450 MeV: Missing Data & Theoretical Expectations

- **No** ^{3}He+C analyzing power data exist anywhere in the literature above $\sim$450 MeV
- Optical model parametrizations (Trost et al., Pang et al.) calibrated below 220–250 MeV — cannot be extrapolated reliably into the Booster range
- **Kinematic concern**: FOM peak shifts to smaller angles $\propto 1/p$
  - At 443 MeV: peak at $\theta \approx 8^\circ$–9°
  - At extraction: shifts to $\sim 3^\circ$–$4^\circ \Rightarrow$ approaching inner edge of forward ring (7.6°)
  - Far-forward ring at $z = 1000$ mm with 50 mm clearance motivated (covers $\theta \geq 3.0^\circ$–3.1°)

Strategy for Determining A_y and Managing Depolarization Resonances

- Spin tune sweeps from -4.193 (injection) to -7.904 (extraction) — crosses 3 imperfection and 2 intrinsic resonances
- AC dipole technique: full spin-flip demonstrated in simulation at intrinsic resonances — partial depolarization cannot be excluded
- **Three complementary strategies for A_y determination**:
  - **Between resonance crossings**: instantaneous P is a known fraction of injection $P \Rightarrow A_y$ directly from asymmetry and known P
  - **Cycle-to-cycle characterisation**: depolarization at each resonance is reproducible $\Rightarrow$ map fractional P remaining after each step by comparing asymmetry before/after each crossing
  - **Calibrated polarization export from 443 MeV anchor**: ramp to target energy, measure asymmetry, return to 443 MeV to verify P survived the excursion (demonstrated at IUCF Cooler Ring)
- Together these make the Booster polarimeter a practical instrument for systematic determination of $^3\mathrm{He}\,\mathrm{C}$ analyzing powers across the full ramp

Conclusion

- **Staged commissioning**: Stage 1 (recoil only) → $p\mathrm{C}$ polarimetry; Stage 2 (add forward ring) → $^3\mathrm{He}\,\mathrm{C}$ polarimetry
- $p\mathrm{C}$ performance: $t_{\mathrm{dwell}} = 3$–15 ms for $\delta P = 10^{-3}$ — four to five orders of magnitude shorter than the 75 ms ramp
- $^3\mathrm{He}\,\mathrm{C}$ at 443 MeV: $t_{\mathrm{dwell}} \approx 1$ s — statistics-free at the anchor energy; above 450 MeV: calibrated export technique and resonance-crossing analysis will bridge the gap
- At extraction the $^3\mathrm{He}\,\mathrm{C}$ FOM peak shifts to $\sim 3°$–$4°$: a far-forward ring at $z = 1000$ mm with 50 mm clearance is motivated
- Blank flanges at $z = 400$ mm for future deuteron polarimetry (vector + tensor) — no impact on current operation
- Motivation:
  - optimize polarization transmission Booster → AGS → EIC
  - Independent polarization measurement between source and AGS
  - Provides independent polarimetry during AGS refurbishment

Fixed-Geometry ^{12}C Recoil Detection for All Five Beam Species

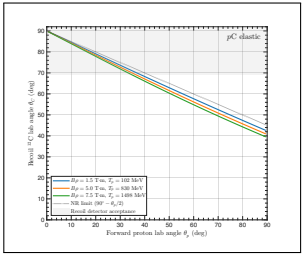

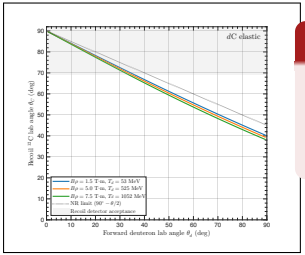

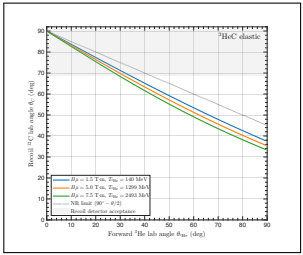

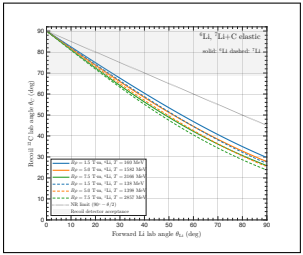

Key result

For forward beam angles up to $\sim 30^\circ$, all five species give recoil ^{12}C at $\theta_C \approx 70^\circ$–$90^\circ$ — a **single fixed recoil ring serves every species across the full Booster ramp.**

- **Five beam species:** p, d, ^{3}He, ^{6}Li, ^{7}Li
- **Weak energy dependence:** curves overlap inside the $\theta_C = 69^\circ$–91° band at all three rigidities for every species
- **Weak species dependence:** despite large mass differences, all curves lie near the billiard limit
- Forward coincidence window ($\theta \lesssim 15^\circ$) within the stable recoil band for all species

$\Rightarrow$ **No mechanical reconfiguration** needed when switching species or energy